A Layered Iron-Rich 2234-Type with a Mixed Valence of Iron: The Ferrimagnetic Tl-Doped $Fe_2(Sr_{2-\epsilon}Tl_\epsilon)Sr_3Fe_4O_{14.65}$

Christophe Lepoittevin,[†] Sylvie Malo,*[,‡] Ninh Nguyen,[‡] Sylvie Hebert,[‡] Gustaaf Van Tendeloo,[†] and Maryvonne Hervieu[‡]

EMAT Laboratory, Antwerpen University, Groenenborgerlaan 171, 2020 Antwerpen, Belgium, and Laboratoire CRISMAT-ENSICAEN, Bd du Maréchal Juin-14050, Caen, Cedex, France

Received May 26, 2008. Revised Manuscript Received July 22, 2008

A new Tl-doped strontium ferrite $Fe_2(Sr_{2-\epsilon}Tl_\epsilon)Sr_3Fe_4O_{14.65}$, with an original structure, has been synthesized and structurally characterized by powder X-ray diffraction and transmission electron microscopy. The TGA and Mössbauer studies evidence a mixed valence of iron. The structure exhibits a commensurate modulation, with a F-type subcell $a \approx b \approx 5.4$ Å ($\approx a_p\sqrt{2}$), $c \approx 42$ Å with a modulation vector $\vec{q} = \alpha\vec{a}^*$ with $\alpha = 0.4$. The supercell parameters have been refined as $a = 27.1101(8)$ Å, $b = 5.5187(2)$ Å and $c = 42.0513(9)$ Å, in the space group *Fmmm*. The electron diffraction and electron microscopy data of this novel ferrite show that it can be described as a Fe_{Tl}-2234-type structure corresponding to the intergrowth of a quadruple perovskite slice $[(SrFeO_{2.8})_4]$, with a complex rock salt related slice $[Fe_2(Sr_{2-\epsilon}Tl_\epsilon)O_{3.4}]_\infty$, built up of one double iron layer $[Fe_2O_{2.4}]$ sandwiched between two [SrO] layers. The HRTEM images show that the oxygen atoms and vacancies are randomly distributed in the perovskite layers while the HAADF STEM images evidence the absence of Tl segregation in the matrix. $Fe_2(Sr_{2-\epsilon}Tl_\epsilon)Sr_3Fe_4O_{14.65}$ exhibits a very large value of χ (11emu/mol) at 5 K, which remains large at 400 K; the M(H) loop presents a shape characteristic of ferrimagnetism, with a large coercive field of 0.3 T. The value of magnetization saturates at 400 K at 0.68 μ_B/Fe. At 10 K, the value of magnetization reaches a maximum of 2 μ_B/Fe. The resistivity presents a semiconducting-like behavior, with $\rho \sim 800$ Ω·cm at 300 K.

Introduction

Transition metal oxides have been investigated with great care since the discovery of the remarkable properties of superconductivity in the cuprates, colossal magnetoresistance in the manganites, or thermoelectricity in the cobaltites. Renewed interest occurred in the iron oxides after evidence of their thermoelectric and multiferroic potential properties. Iron-based systems are indeed the source of a rich chemistry because of the variety of coordination environments possible for iron and the range of its oxidation states, from +2 to +4, both easily accessible in perovskite-related structures. Sr−Fe−O is one example of an exceptionally rich system with the existence of three important structural families. The iron atoms adopt IV, V, and VI coordination in the oxygen deficient perovskites $SrFeO_{3-x}$.[1−6] The same effect takes place in the layered Ruddlesden−Popper (RP) phases $Sr_{m+1}Fe_mO_{3m+1}$,[7,8] built up from an intergrowth of one rock salt-type [SrO] layer with m $[SrFeO_{3-y}]$ perovskite layers. The complex oxide $Sr_4Fe_6O_{13}$[9,10] has also been the subject of numerous papers describing its properties, because of its application in the field of oxygen-selective membranes. Electron diffraction studies recently evidenced that the origin of the complexity is the modulated character of the structure, clearly associated to the oxygen stoichiometry.[11,12] The structure of the oxygen deficient $Sr_4Fe_6O_{13-\delta}$ compounds can be described as an intergrowth of one perovskite layer $[SrFeO_{3-y}]$ with a rock salt (RS) derivative block, made of a complex double iron layer sandwiched between two [SrO] layers. In these oxides, the iron atoms adopt four types of coordination.

In the present paper, we report a novel thallium-doped ferrite. Its structure is directly related to that of the $Sr_4Fe_6O_{13-\delta}$ and $SrFeO_{3-y}$ oxides. This Tl-doped strontium ferrite with approximate composition $Fe_2(Sr_{1.9}Tl_{0.1})Sr_3Fe_4O_{14.65}$ has been structurally characterized by powder X-ray diffraction and electron microscopy, and its magnetotransport properties have been investigated. This study allows to enlarge the

* Corresponding author. E-mail: sylvie.malo@ensicaen.fr.
[†] Antwerpen University.
[‡] Laboratoire CRISMAT-ENSICAEN.

(1) Bertaut, E. F.; Blum, P.; Sagnieres, A. *Acta Crystallogr.* **1959**, *12*, 149.
(2) Takeda, Y.; Kanno, K.; Takada, T.; Yamamoto, O.; Takano, M.; Nakayama, N.; Bando, Y. *J. Solid State Chem.* **1986**, *63*, 237.
(3) Grenier, J. C.; Pouchard, M.; Hagenmuller, P. *Struct. Bonding (Berlin, Ger)* **1981**, *141*, 1.
(4) Grenier, J. C.; Ea, N.; Pouchard, M.; Hagenmuller, P. *J. Solid State Chem.* **1985**, *58*, 243.
(5) Takano, M.; Okita, T.; Nakayama, N.; Bando, Y.; Takeda, Y.; Yamamoto, O.; Goodenough, J. B. *J. Solid State Chem.* **1988**, *73*, 140.
(6) Hodges, J. P.; Short, S.; Jorgensen, J. D.; Xiong, X.; Dabrowski, B.; Mini, S. M.; Kimball, C. W. *J. Solid State Chem.* **2000**, *151*, 190.
(7) Adler, P. *J. Solid State Chem.* **1994**, *108*, 275.
(8) Prado, F.; Mogni, L.; Cuello, G. J.; Caneiro, A. *Solid State Ionics* **2007**, *178* (1−2), 77.
(9) Yoshiasa, A.; Ueno, K.; Kanamaru, F.; Horiuchi, H. *Mater. Res. Bull.* **1986**, *21*, 175.
(10) Ohkawa, M.; Fujita, S.; Takeno, S.; Nakatsuka, A.; Yoshiasa, A.; Uchida, M.; Oshumi, K. *Z. Kristallogr.* **1997**, *212*, 848.
(11) Mellenne, B.; Retoux, R.; Lepoittevin, C.; Hervieu, M.; Raveau, B. *Chem. Mater.* **2004**, *16*, 5006.
(12) Rossel, M. D.; Abakumov, A. M.; Van Tendeloo, G.; Pardo, J. A.; Santiso, J. *J. Chem. Mater.* **2004**, *16*, 2578.

10.1021/cm8014385 CCC: $40.75
Published on Web 09/25/2008

Table 1. Layered Phases Stabilized in the A-Rich and Fe-Rich Parts of the A−Sr−Fe−O Systems

formulation	(n, m)	$(n-1)2(m-1)m$	references
	A-Rich Part		
$(Sr_2)FeO_{4-x}$	$(n = 1, m = 0)$	"0201"	7−14
$(Bi_{0.4}Sr_{0.5})(Sr_2)FeO_5$	$(n = 2, m = 1)$	Bi-1201	15
$Tl(Sr_2)SrFe_2O_8$	$(n = 2, m = 2)$	Tl-1212	16
$(Bi_{2-x}Sr_x)(Sr_2)FeO_{6+\delta}$	$(n = 3, m = 1)$	Bi-2201	17
$(Bi_2)(Sr_{2-x}Bi_x)SrFe_2O_{9+\delta}$	$(n = 3, m = 2)$	Bi-2212	18, 19
$Bi_2(Sr_2)Sr_2Fe_3O_{12}$	$(n = 3, m = 3)$	Bi-2223	20, 21
	Fe-Rich Part		
$(Fe_2)(Sr_2)FeO_{6.5-\delta/2}$	$(n = 3, m = 1)$	Fe-2201	11−23
$Fe_2(Bi_{0.69}Sr_{1.31})SrFe_2O_{9.33}$	$(n = 3, m = 2)$	Fe_{Bi}-2212	24
$Fe_2(Sr_{1.9}Tl_{0.1})Sr_3Fe_4O_{14.65}$.	$(n = 3, m = 4)$	Fe_{Tl}-2234	this work

structural family of ferrites and to evidence its ferrimagnetic behavior with a mixed valence of iron.

Structural (Re)considerations. In the search for new superconducting high Tc (HTSC) cuprates and its derivatives,[13] other large structural families have been discovered, which are characterized by different numbers n of rock salt-type layers ($n = 1$, $n = 2$ and 3) and m of perovskite-type d^{10} cation (mainly $A = Bi^{3+}$ and Tl^{3+}) in the system. In the $n = 2$ member, the rock salt block consists of one intermediate [AO] layer sandwiched between two [SrO] layers, and for the $n = 3$ member, two intermediate [AO] layers are sandwiched between two [SrO] layers. A simple notation, based on the sequence of the cation indices $(n-1)2(m-1)m$, has been adopted by the community to denote these materials; some examples of strontium-based ferrites are collected in Table 1.

In the iron rich part of the Sr−Fe−O based diagram (Table 1), the structural analyses of $Sr_4Fe_6O_{13-\delta}$ allow description of the framework as the intergrowth of one perovskite layer [$SrFeO_3$] ($m = 1$) with a rock salt (RS)-type block ($n = 3$) made of one complex double iron layer [$Fe_2O_{2.5-\delta/2}$], sandwiched between two [SrO] layers. According to this description, $Sr_4Fe_6O_{13-\delta}$ belongs to the 2201-type members (Figure 1); it will be denoted Fe-2201. Its formulation can therefore be written as $(Fe_2)(Sr_2)FeO_{6.5-\delta/2}$, which highlights two structural particularities: the double intermediate layer of the RS block, which contains only transition metals (instead of $5d^{10}$ cations, Bi, Tl, Pb, or Hg in the HTSCs) and the presence of an excess of oxygen as in the double bismuth layers of the HTSCs.[13] The second member of the family, characterized by a double perovskite layer ($m = 2$), $Fe_2(Bi_{0.69}Sr_{1.31})SrFe_2O_{9.33}$, is denoted Fe_{Bi}-2212 in order to outline the structural difference with other 2212-type Bi rich structures, which exist in the Bi−Sr−Fe-O system, namely the $(Bi_{2-x}Sr_x)(Sr_2)FeO_{6+\delta}$ phases,[19] denoted Bi-2212's.

The refinement of the incommensurate modulated structure[22] from single crystal data allowed the different environments to be determined for the iron cations located in the double [$Fe_2O_{2.5-\delta/2}$] layer. They are tetragonal pyramids (TP), monocapped tetrahedra (MT), and trigonal bipyramids (TBP), which are combined in groups of two or three to form three basic structural units: [(TP)(TP)], [(TP)(MT)(TP)], and [(TBP)(TBP)] (Figure 1). Note that the [(TBP)(TBP)] basic structural unit plays a peculiar role since one additional oxygen atom is located at the junction of the two adjacent trigonal bipyramids, in between the two [FeO] planes of the double layer. This basic structural unit systematically alternates with either the [(TP)(TP)] or [(TP)(MT)(TP)], depending on the component of the modulation vector.[22] In the Fe-rich 2212's member, $Fe_2(Bi_{0.69}Sr_{1.31})SrFe_2O_{9.33}$[24] denoted Fe_{Bi}-2212, the double iron layers of the RS block follow a similar mechanism but differ by the nature of the second basic structural unit, made of four polyhedra [(TP)-(MT)(MT)(TP)], which alternates with the [(TBP)(TBP)] basic structural unit previously determined.

In the present paper, the Tl-doped iron rich 2234-type strontium ferrite $Fe_2(Sr_{1.9}Tl_{0.1})Sr_3Fe_4O_{14.65}$ with a quadruple perovskite layer will be denoted Fe_{Tl}-2234.

Experimental Section

Different batches of powder samples have been prepared from mixtures of Tl_2O_3, SrO (and SrO_2 to increase the partial pressure of oxygen in the sealed tube), and Fe_2O_3, according to the general formula $Fe_2(Sr_{2-x}Tl_x)Sr_3Fe_4O_{14+1/2x+z}$. These oxides have been ground in an agate mortar in order to obtain a homogeneous powder, pressed into pellets, introduced in alumina crucibles, and sealed in silica tubes; last, the sealed tube was introduced in an alumina tube in order to avoid thallium oxide contamination in case it should explode. The mixtures were heated at 1100 °C for 48 h, followed by a cooling rate of 3 °C/min. The powder X-ray diffraction (PXRD) was performed at room temperature with a Philips diffractometer equipped with a Cu Kα radiation ($\bar{\lambda} = 1.54181$Å) in the range $10° \leq 2\theta \leq 110°$.

Specimens for transmission electron microscopy (TEM) were prepared by crushing a small piece of the sample in an agate mortar containing ethanol and dropping a droplet on a copper grid covered by a holey carbon film. The electron diffraction (ED) investigation and the energy dispersive spectroscopy (EDS) analyses were carried out with a Philips CM 20 microscope equipped with a ±45° and ±30° double tilt. The microscope used for the high resolution electron microscopy (HRTEM) was a JEOL 4000EX operating at 400 kV. The *Z*-contrast images were obtained on a JEOL 3000F microscope equipped with a scanning (STEM) unit and a high-angle annular dark field (HAADF) detector. High resolution images were simulated using the Mac Tempas software.

The magnetic measurements were performed by SQUID magnetometry ($T < 400$ K). The resistivity measurements were carried out by the four-probes method on a Physical Properties Measurements System (PPMS).

The ^{57}Fe transmission Mössbauer spectrum for the powder sample was measured at 80 K using a ^{57}Co/Rh source. The spectrum has been simulated using a least-squares fitting routine assuming a Lorentzian line shape called MOSFIT ("MOSFIT" unpublished

(13) Raveau, B.; Michel, C.; Hervieu, M.; Groult, D. *Crystal chemistry of High Tc superconducting copper oxides. Springer Series in Materials Science 15*; Springer-Verlag: Dusseldorf, 1991.
(14) Dann, S. E.; Weller, M. T.; Currie, D. B. *J. Solid State Chem.* **1991**, *92*, 237.
(15) Allix, M.; Pelloquin, D.; Studer, F.; Nguyen, N.; Wahl, A.; Maignan, A.; Raveau, B. *J. Solid State Chem.* **2002**, *167*, 48.
(16) Daniel, P.; Barbey, L.; Nguyen, N.; Ducouret, A.; Groult, D.; Raveau, B. *J. Phys. Chem. Solids* **1994**, *55* (9), 795.
(17) Pelloquin, D.; Allix, M.; Michel, C.; Hervieu, M.; Raveau, B. *Phil. Mag. B* **2001**, *81*, 1669.
(18) Lepage, Y.; Mc Kinnon, W. R.; Tarascon, J. M.; Barboux, P. *Phys. Rev. B* **1989**, *40*, 6810.
(19) Hervieu, M.; Michel, C.; Nguyen, N.; Retoux, R.; Raveau, B. *Eur. J. Solid State Inorg. Chem.* **1988**, *25*, 375.
(20) Retoux, R.; Michel, C.; Hervieu, M.; Nguyen, N.; Raveau, B. *Solid State Commun.* **1989**, *69*, 599.
(21) Pissas, M.; Papaefthymiou, V.; Simopoulos, A.; Kostikas, A.; Niarchos, D. *Solid State Commun.* **1990**, *73*, 767.

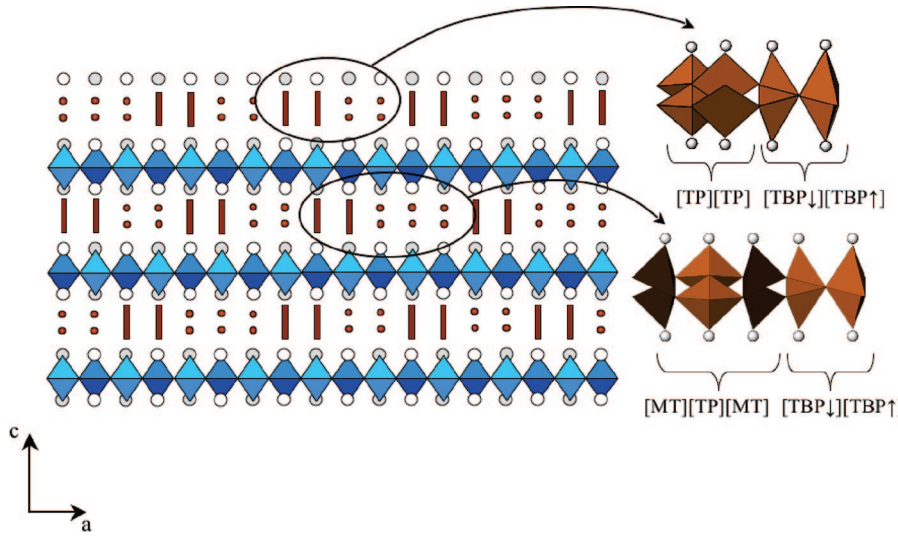

Figure 1. Idealized projection of the structural model of the Fe-2201: $Sr_4Fe_6O_{13-\delta}$. The FeO_6 octahedra are represented by diamonds and the Sr (and Tl) atoms by open circles whereas the double iron layers are schematically drawn as sequences of two sticks alternating with two or three double dots. The corresponding structural units of the complex double iron layer are drawn in the right part of the figure.

program, F. Varret, J. Teillet, Université du Maine, France). The isomer shifts (IS) are corrected for the room temperature IS of metallic iron taken as a reference.

Results

The analysis of the samples was first carried out by combining XRPD and electron diffraction data. This first investigation of the Tl−Sr−Fe−O diagram evidenced the existence of a 2234-type phase. For an ideal 2234-type compound, the stoichiometric formula is $A_2(A'_2)A''_3B_4O_{15}$ (A, A′, and A″ being the large cations of the RS blocks and perovskite cages and B the transition metal). Considering the peculiar modulated character of the present family and the formulation of the complex double iron layer [$Fe_2O_{2.5-\delta/2}$] on the one hand, and the possible oxygen deficiency of the perovskite layer [$SrFeO_{3-y}$] on the other hand, the theoretical formula of the expected phase can be written as $(Fe_2)(Sr_{2-x}Tl_x)Sr_3Fe_4O_{15.5-\delta/2-4y}$.

X-ray diffraction analysis (Figure 2a) showed that the 2234-type phase is only obtained when the synthesis is performed, starting with SrO as a source of Sr and an excess, followed by a loss, of thallium oxide deposited on the container walls. The samples appear in the form of bars, with black crystallites.

Chemical Analysis. The EDS coupled with ED analyses, carried out on numerous crystallites revealed a main phase with an average Sr/Fe ratio close to 0.83 and the presence of $Sr_4Fe_6O_{13-\delta}$ as the only minority phase (less than 5% of the crystallites).

The average content of thallium in the new phase is estimated to 2% of the Sr content in the limit of accuracy of the technique. The analyses were carried out on several tens of crystallites; the standard deviation of Tl content is $Tl_{0.1\pm0.04}$.

Results of cerimetric titration analyses, carried out on several samplings, cannot be considered definitely reliable because of the imperfect solubility of the sample.

The TGA, carried out in a mixture 10% H_2/Ar at 400 °C,[25] evidenced a mixed valence of iron with an oxygen content close to 14.7 per unit, leading to a calculated valence of iron close to 3.22.

In order to confirm the valence state of the iron ions, the ^{57}Fe transmission Mössbauer spectrum for the powder sample was measured at 80 K. Figure 2b shows that the obtained spectrum is rather complex. This agrees with the existence of several iron sites observed in the structural study (see further).

The best fit of this spectrum (Figure 2b) requires five Mössbauer magnetic sextuplets noted as A, B, C, D, E and an additional small paramagnetic doublet (about 4% of relative intensity) which could be from a paramagnetic Fe-based impurity in the compound. The hyperfine parameters of all fitted Mössbauer sites are given in Table 2. The IS and the hyperfine field (H_f) values of the three A, B, and C components (0.32 mm/s ≤ IS ≤ 0.45 mm/s; 51.0 T ≤ H_f ≤ 54.8 T) are typical of trivalent iron ions. While for the D and E sites, the IS and H_f values (IS = −0.02 and −0.01 mm/s; H_f = 31 and 21 T, respectively) indicate that they correspond to Fe^{4+} sites. The relative intensities of different Mössbauer components obtained by the spectrum simulation show that about 80% of iron ions in the compound are in the trivalent state and about 20% are in the tetravalent one.

Additionally, the Mössbauer spectrum confirms the magnetic behavior of the compound at this temperature. This result is in agreement with the TGA measurements, within the accuracy limits of the techniques, and leads to a general formula $Fe_2(Sr_{1.9}Tl_{0.1})Sr_3Fe_4O_{14.65}$ for the new Fe_{Tl}-2234 phase.

(22) Pérez, O.; Mellenne, B.; Retoux, R.; Raveau, B.; Hervieu, M. *Solid State Sci.* **2006**, *8*, 431.
(23) Rossel, M. D.; Abakumov, A. M.; Van Tendeloo, G.; Lomakov, M. V.; Istomin, S. Y.; Antipov, E. *Chem. Mater.* **2005**, *17*, 4717.
(24) Grebille, D.; Lepoittevin, C.; Malo, S.; Pérez, O.; Nguyen, N.; Hervieu, M. *J. Solid State Chem.* **2006**, *179*, 3849.
(25) Hodges, J. P.; Short, S.; Jorgensen, J. D.; Xiong, X.; Dabrowski, B.; Mini, S. M.; Kimball, C. W. *J. Solid State Chem.* **2000**, *151*, 190.

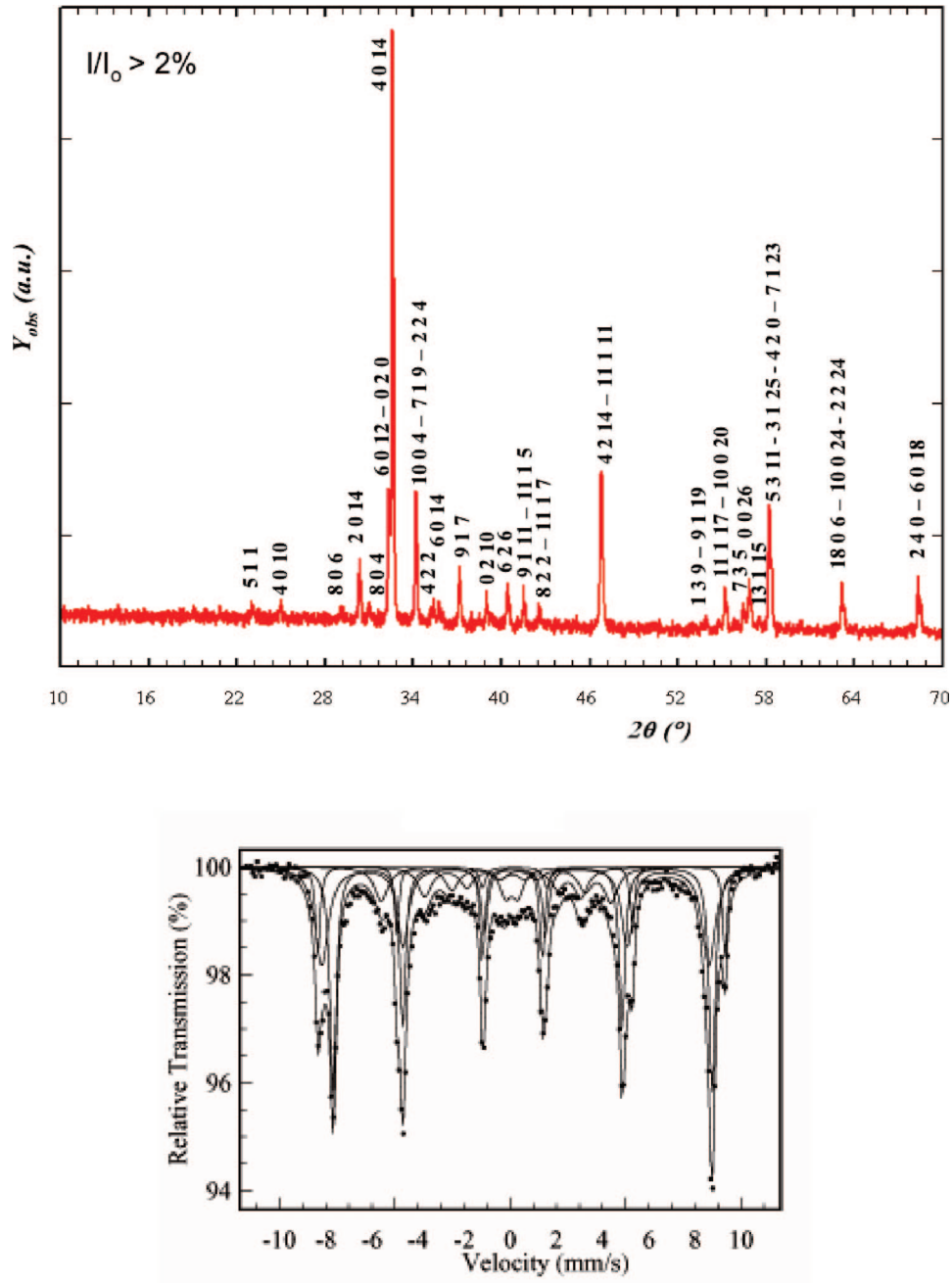

Figure 2. Fe_{Tl}-2234: (a) Powder X-ray diffraction pattern indexed in the super cell (S.G. *Fmmm*) and (b) Mössbauer spectrum recorded at 80 K.

Electron Diffraction and Powder X-ray Diffraction. The reconstruction of the reciprocal space, carried out by tilting around the major crystallographic axes, allowed the determination of the cell parameters and the conditions limiting the reflections (Figure 3a and 3b). Two systems of reflections can be evidenced on the electron diffraction patterns. A first set of intense spots defines an orthorhombic subcell with $a \approx b \approx 5.4$ Å ($\sim a_p\sqrt{2}$), $c \approx 42$ Å (the subscript p is associated to the perovskite unit cell), and the reflection conditions corresponding to a F-type lattice are consistent with the *Fmmm*, *Fmm*2, or *F*222 space group. Besides these fundamental reflections, weaker extra reflections characteristic of a modulated structure are observed in the [010] and [001] ED patterns (Figure 3a and 3b). The modulation vector is $\vec{q} = \alpha\vec{a}^*$ with $\alpha = 0.4$, which implies a commensurate modulation with the superspace group *Fmmm* (α 00)000. Because of the rational value of α, the structure can alternatively be described in a 5-fold supercell with $a = 5a_p\sqrt{2} \approx 27$ Å with *Fmmm* as possible space group; the [100] ED pattern is represented in Figure 3d.

Lattice parameters were refined from the powder X-ray diffraction pattern with the whole pattern matching mode using the Le Bail method with the *Fmmm* space group. The minority phase $Sr_4Fe_6O_{13-\delta}$ (estimated to a few percent by TEM study), not detected by XRPD, was not taken into account for the refinement. The XRPD pattern is given in Figure 2a where only the reflections with $I/I_0 > 2\%$ are indexed. These cell parameters were refined to $a = 27.1101(8)$ Å, $b = 5.5187(2)$ Å, and $c = 42.0513(9)$ Å. However, despite the numerous diffraction peaks characteristic of the supercell, the PXRD data were not sufficient for refining a structural model using the Rietveld method because of their weak

Table 2. Hyperfine Parameters Estimated from the Mössbauer Spectrum of the $Fe_2(Sr_{1.9}Tl_{0.1})Sr_3Fe_4O_{14.65}$Sample at 80 K

IS ± 0.01 (mm/s)	$2\varepsilon^a$ ± 0.01 (mm/s)	H_f ± 0.1 (T)	relative intensity% ± 1	Fe site
0.45	0.29	54.8	10	A/Fe^{3+}
0.32	0.01	52.1	32	B/Fe^{3+}
0.43	0.45	51.0	34	C/Fe^{3+}
−0.02	−0.97	31.0	11	D/Fe^{4+}
−0.01	−0.40	21.0	9	E/Fe^{4+}
0.17	0.54	-	4	paramagnetic impurity

[a] 2ε: quadrupole shift or quadrupolar splitting for the paramagnetic component.

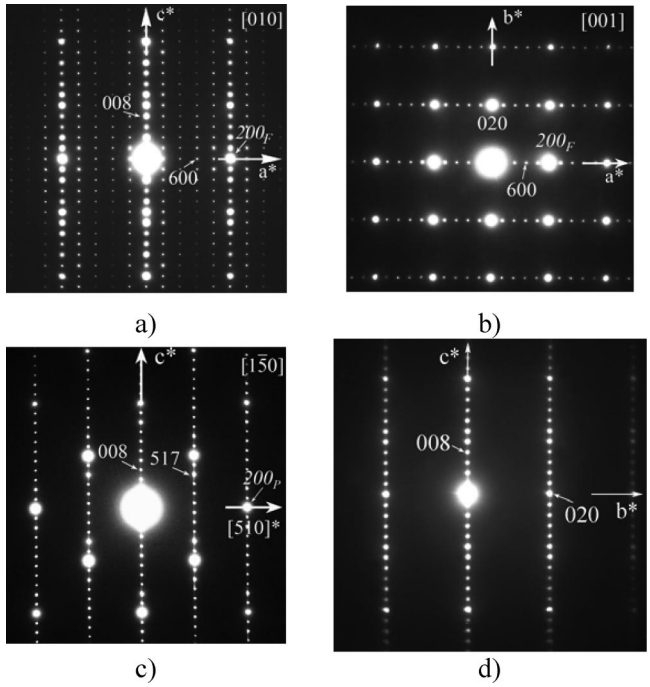

Figure 3. (a) [010], (b) [001] (c) [1$\bar{5}$0] (or $[100]_p$), and (d) [100] ED patterns of Fe_{Tl}-2234 indexed in a F-type supercell. The subscript F refers to the indices in the subcell.

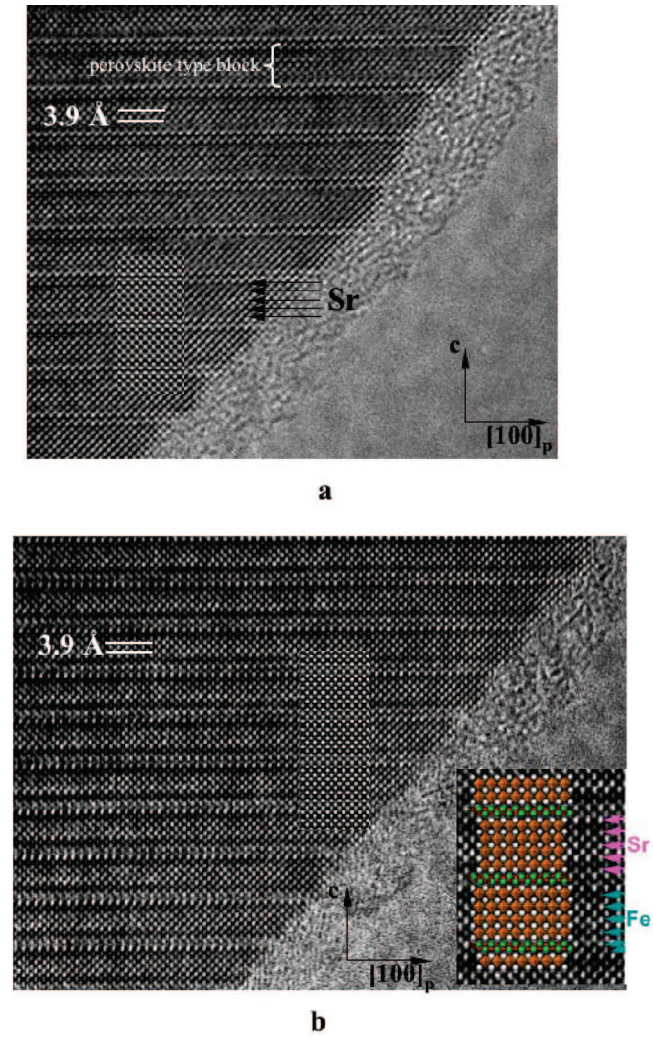

Figure 4. [1$\bar{5}$0] HRTEM images for Fe_{Tl}-2234 recorded for focus values close to (a) −275 Å and (b) −775 Å.

intensity and the huge number of independent crystallographic parameters.

High Resolution Electron Microscopy. *Layers Stacking Mode.* $[100]_p$-oriented HRTEM images are very efficient for the determination of the stacking sequence in intergrowth structures such as Ruddlesden−Popper phases and superconducting cuprates and derivatives[9] as well as for the characterization of the modulated structures. In the present phase, this important $[100]_p$ orientation corresponds to the [1$\bar{5}$0] orientation of the new phase; the corresponding ED pattern is given in Figure 3c. The two images in Figure 4a and 4b display opposite contrasts, corresponding to focus values of −275 Å and −775 Å, respectively. The first image (Figure 4a), in which dark dots are associated to the high electron density zones, shows a regular stacking of nine rows spaced by approximately 1.9 Å ($\approx a_p/2$) in zones corresponding to the characteristic perovskite-type contrast. The dark dots are related to the strontium and iron positions in the perovskite layers. These positions appear as bright dots in Figure 4b, where the high electron density zones are highlighted (see the enlargement in the lower right corner of the HRTEM). These HRTEM images fit with the ones calculated based on a structure described as an intergrowth of a quadruple perovskite layer with a complex double [FeO] layers sandwiched between two [SrO] layers. Note that the contrast at the level of the perovskite layers, viewed along that direction is highly regular, suggesting that there is no local phenomena associated to the iron polyhedra distortion or oxygen/vacancy short-range ordering.

To understand the nonstoichiometric mechanisms associated to the superstructure formation in these different layers and to propose a valuable structural model, the [010]-oriented HRTEM images are essential. The previous studies carried out on the derivative structures, Fe-2201's[11,12,22,23] and Fe_{Bi}-2212's,[24] which exhibit incommensurate and commensurate modulations, provide important information on the stacking layer regularity (as almost any [*hk0*] HRTEM image) and on the nature of the modulation. Two typical [010] HRTEM images of the Fe-2201's (Figure 5a) and Fe_{Bi}-2212's (Figure 5b) phases are compared to those observed for the present phase (Figure 5c). The contrast at the upper part of the figures corresponds to the high electron density as bright dots, while the contrast at the lower part shows the high electron density as dark dots. In the three upper images, the $[SrO]_\infty$ layers appear as rows of bright dots. The common characteristic to the three phases is the slice, bordered by two $[SrO]_\infty$ layers and 5.6 Å thick corresponding to a

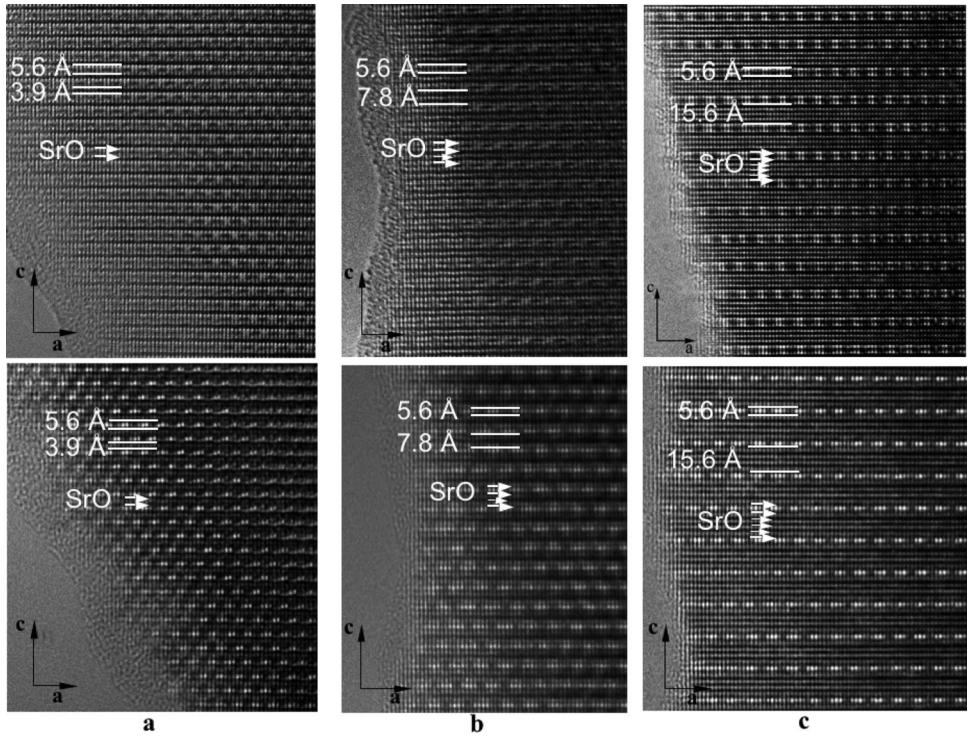

Figure 5. The upper [010] HRTEM images correspond to high electron density contrasts and the lower images to the weak electron density contrast. The series compare (a) Fe-2201 ($Fe_2(Sr_2)Fe_2O_{6.46}$), (b) Fe_{Bi}-2212 ($Fe_2(Bi_{0.69}Sr_{1.31})SrFe_2O_{9.33}$), and (c) Fe_{Tl}-2234 ($Fe_2(Sr_{1.9}Tl_{0.1})Sr_3Fe_4O_{14.65}$).

complex rock salt-type block. In between, one observes respectively: one dark row (3.9 Å thick) associated to one "octahedral" [FeO_{2-y}] layer of the perovskite slice for the 2201's, one row of bright dots sandwiched between two [FeO_{2-y}] layers (7.8 Å thick) for the 2212's and three rows of bright dots sandwiched between four [FeO_{2-y}] layers (15.6 Å thick) for the new phase, in agreement with the hypothesis of a 2234-type phase. Imaging along these different directions confirms the regularity at the level of the perovskite layers.

Rock Salt-Type Block. The complex variations of contrast along $\vec{a}$ at the level of the rock salt-type slice, 5.6 Å thick, are clearly observed in the images of the three phases (Figure 5). The previous studies of the Fe-2201's[22] and Fe_{Bi}-2212's,[24] which allowed a direct correlation between the image and the iron environments, gave us the key to decode these variations (shown in Figure 6a for the HRTEM image recorded for one Fe-2201). The images indeed show that, depending on the focus value, the [(TBP)(TBP)] basic structural unit, which contains the additional oxygen atom, exhibits a characteristic contrast, as the alternating units of two ([(TP)(TP)]), three ([(TP)(MT)(TP)]), or four ([(TP)-(MT)(MT)(TP)]) polyhedra.

The sequence along $\vec{a}$ of the present phase (Figure 6b) consists of a regular alternation of two bright sticks spaced by 2.8 Å with three less bright dots. As a consequence, based on the observations and calculations carried out on the Fe-2201 and Fe_{Bi}-2212 ferrites,[22−24] a model can be proposed. The 2:3 sequence is associated with a double distorted edge sharing trigonal bipyramids row [(TBP)(TBP)] alternating along $\vec{a}$ with two monocapped tetrahedra surrounding one distorted tetragonal pyramid [(MP)(TP)(MP)] (Figure 7). From this model, as previously for the Fe-2201 phases,[22] the α value determined by ED can be directly linked to the

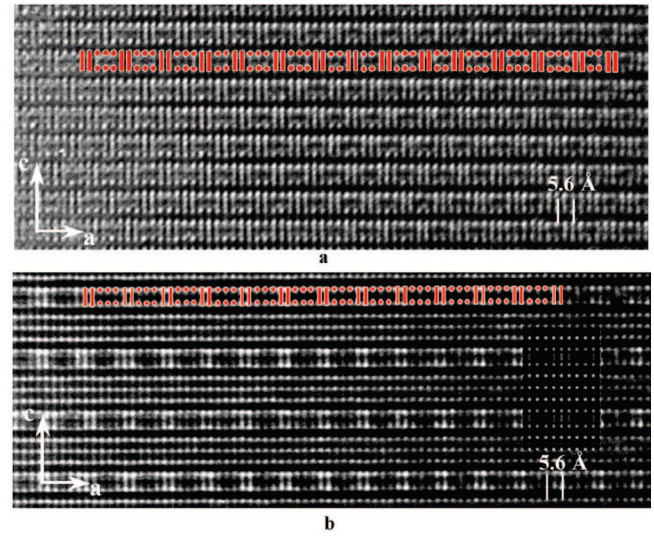

Figure 6. [010] HRTEM images for (a) Fe-2201 and (b) Fe_{Tl}-2234.

number of extra oxygen atoms (per unit cell) in the rock salt-type slice through the relation $\delta = 1 - 2\alpha$.

Taking this consideration into account, the description of the new phase $Fe_2(Sr_{1.9}Tl_{0.1})Sr_3Fe_4O_{14.65}$ as a Fe_{Tl}-2234-type structure can be completed. With the knowledge of the modulation vector, we proposed a model (Figure 7) and a composition for the complex triple rock salt-related layer: $[Fe_2(Sr_{1.9}Tl_{0.1})O_{3.4}]_\infty$. According to the overall oxygen content ($O_{14.65}$) and the one of the RS block ($O_{3.5-\delta/2} = O_{3+\alpha}$), i.e. $O_{3.4}$, the composition of one perovskite slice can be easily calculated, namely $[(SrFeO_{2.8})]_\infty$. $Fe_2(Sr_{1.9}Tl_{0.1})Sr_3Fe_4O_{14.65}$ is therefore built up as a regular alternation along $\vec{c}$ of a complex triple rock salt-related layer $[Fe_2(Sr_{1.9}Tl_{0.1})O_{3.4}]_\infty$ with a quadruple perovskite slice $[(SrFeO_{2.8})_4]_\infty$.

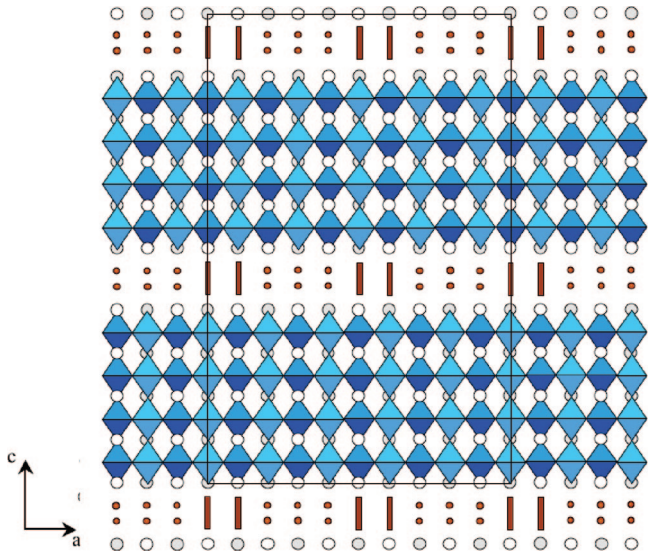

Figure 7. Structural model of the novel phase Fe_{Tl}-2234.

Scanning Transmission Electron Microscopy. The different layers of the Fe-2201 parent structure are occupied by only two cations, either Sr or Fe, no long-range ordered phase has been stabilized in this system at the present time and it is of interest to understand the way the $5d^{10}$ cations are arranged in these layered structures. The high-angle annular dark field (HAADF) scanning electron microscopy (STEM) is the appropriate technique for such a study. In this mode, the intensity related to a column of atoms is proportional to Z^n (with $1 < n < 2$), where Z is the average atomic number of the projected column. In other words, in Z-contrast, the higher Z the element will get, the brighter the dot on the image is. In the present family, we have two different members for carrying out this study, the Fe_{Bi}-2212's and Fe_{Tl}-2234's. For the Fe_{Bi}-2212's, $Fe_2(Bi_{0.69}Sr_{1.31})$-$SrFe_2O_{9.33}$, it is an important test because the X-ray diffraction study on single crystal has demonstrated that bismuth and strontium atoms are randomly distributed in the strontium site at the periphery of the double perovskite layer,[24] the strontium site situated at the center being full strontium-occupying sites.

The [010] HAADF STEM image of (Fe_{Bi}-2212) in Figure 8a exhibits two rows of brights dots spaced by 7.8 Å, associated to the projection of Bi and Sr columns, and a single row of weaker dots in between, corresponding to the projection of Sr columns. HAADF STEM images oriented along [010] and [1$\bar{5}$0] for Fe_{Tl}-2234's (Figure 8b and 8c, respectively) show five bright rows in the 15.6 Å thick quadruple perovskite layer, but none of these rows displays such a high contrast difference as the one for Fe_{Bi}-2212. This observation, which is in agreement with the low thallium content determined by the EDS analyses in this Fe_{Tl}-2234 structure, evidences the absence of its possible "clustering" in the form of "Tl-rich" phases, where Tl cations would occupy the intermediate layers of the rock salt layers. Note that the waviness of the layers is not a real effect but induced in STEM by the instability of the sample during the recording.

Nonstoichiometry Mechanisms. The HRTEM investigation also revealed the appearance of crystallographic shear planes

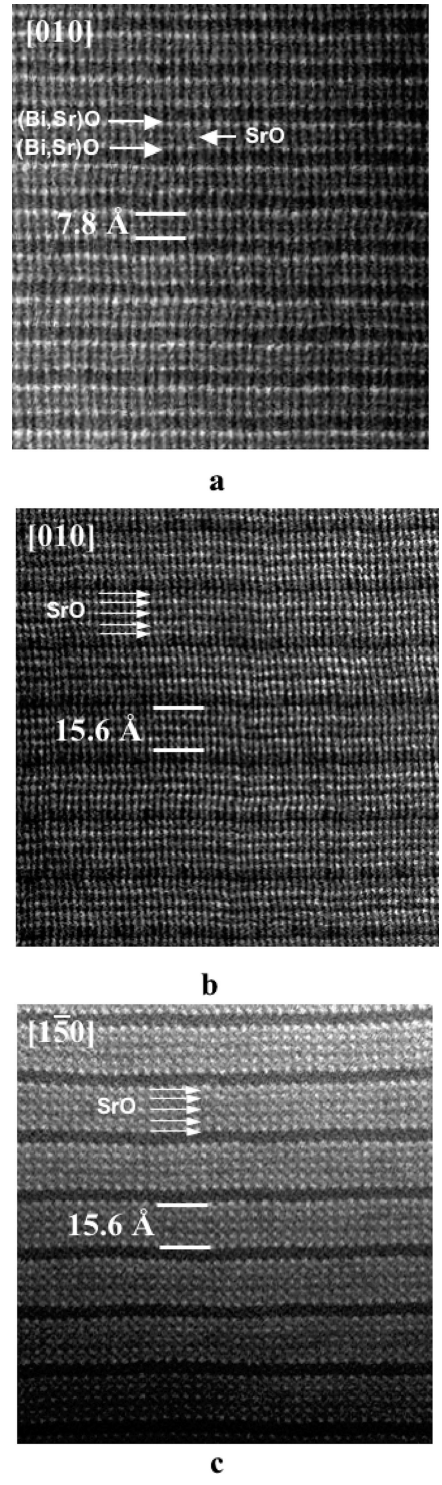

Figure 8. [010] HAADF STEM image for (a) Fe_{Bi}-2212 ($Fe_2(Bi_{0.69}Sr_{1.31})$-$SrFe_2O_{9.3}$), (b) Fe_{Tl}-2234 ($Fe_2(Sr_{1.9}Tl_{0.1})Sr_3Fe_4O_{14.65}$), and (c) [1$\bar{5}$0] HAADF STEM image for Fe_{Tl}-2234.

as a nonstoichiometry mechanism. Shear planes frequently appear as defects in oxygen deficient ReO_3 and perovskite-related structures.[26] The mechanism is commonly engaged by oxygen deficiency or/and by the introduction of large cations. There are several examples of "collapsed" (or "terrace") structures generated by such shear mechanisms in perovskite related phases with transition metals. In the

(26) Wells, A. F. *Structural Inorganic Chemistry*, 5th ed.; Clarendon Press: Oxford, 1984.

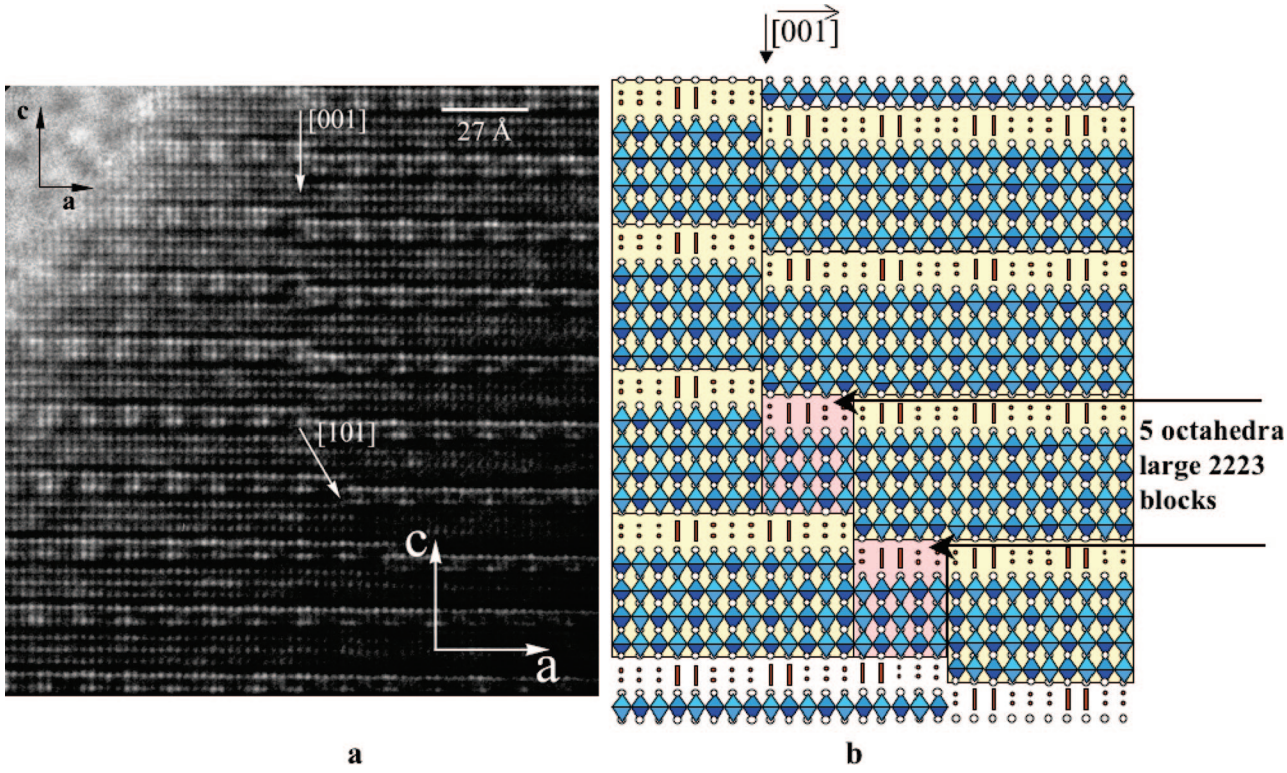

Figure 9. (a) [010] HREM image for Fe_{Tl}-2234 showing shearing planes and (b) their schematically structural representation.

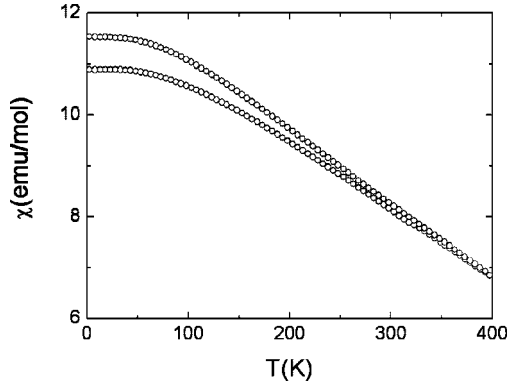

Figure 10. Fe_{Tl}-2234: $\chi(T)$ measured under a magnetic field of 0.3 T in zero-field cooling and field-cooling modes.

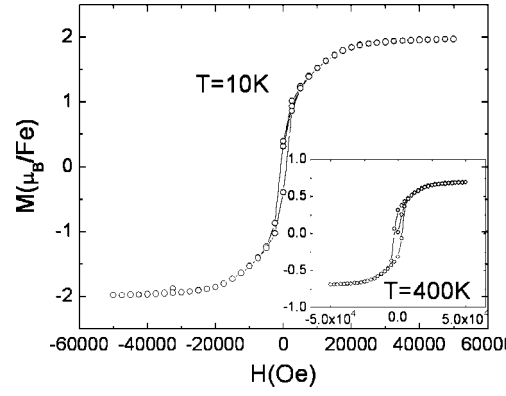

Figure 11. Fe_{Tl}-2234: M(H) at 10 K and 400 K (inset).

Fe-based systems, examples have been observed with Birich phases,[27−29] with Fe-rich phase[30] and perovskite.[31] The [010] HRTEM image in Figure 9a exhibits one of these crystallographic shear planes, and its schematic representation is given in Figure 9b. The shearing appears to take place along two different planes: one along the $(001)_{2234}$ plane, the other along the $(101)_{2234}$ plane involving the insertion of five octahedra large 2223-type bricks.

Magnetic and Transport Properties. Figure 10 presents the susceptibility measured up to 400 K under 0.3 T. The ZFC and FC curves decrease as T increases and are separated over almost the whole T range. The value of χ is very large (11emu/mol) at 5 K) and remains large at 400 K, suggesting that the transition temperature of this material is above 400 K.

M(H) loops presented in Figure 11 confirm that the transition temperature is above 400 K. At 400 K, the M(H) loop presents a shape characteristic of ferro- or ferrimagnetism, with a coercive field of 0.3T. The value of magnetization saturates at 400 K at 0.68 μ_B/Fe. At lower T, i.e. $T = 10$ K in Figure 11, the value of magnetization is larger and reaches a maximum of 2 μ_B/Fe. However, the coercive field is lower for that temperature which is not expected for a typical ferro-or ferrimagnetic compound. Considering that the moment for Fe^{3+} and Fe^{4+} corresponds respectively to 5 μ_B and 4 μ_B, the smaller value of 2 μ_B/Fe suggests that a ferrimagnetic ordering could be obtained in Fe_{Tl}-2234's.

(27) Hervieu, M.; Caldes, M. T.; Michel, C.; Pelloquin, D.; Raveau, B. *J. Solid State Chem.* **1995**, *118*, 357.
(28) Hervieu, M.; Pérez, O.; Groult, D.; Grebille, D.; Leligny, H.; Raveau, B. *J. Solid State Chem.* **1997**, *129*, 214.
(29) Pérez, O.; Leligny, H.; Baldinozzi, G.; Grebille, D.; Hervieu, M.; Labbe, P.; Groult, D.; Graafsma, H. *Phys. Rev. B* **1997**, *56*, 5662.
(30) Lepoittevin, C.; Malo, S.; Pérez, O.; Nguyen, N.; Maignan, A.; Hervieu, M. *Solid State Sci.* **2006**, *8*, 1294.
(31) Abakumov, A. M.; Hadermann, J.; Bals, S.; Nokolaev, I. V.; Antipov, E. V.; van Tendeloo, G. *Angew. Chem.* **2006**, *45*, 6697.

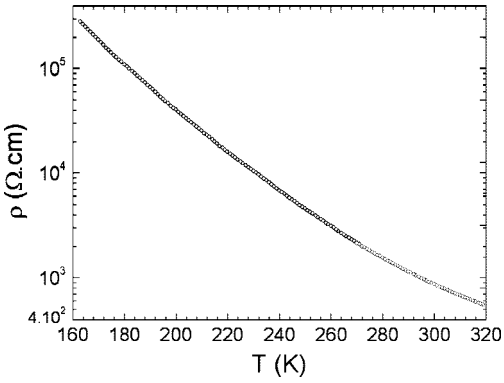

Figure 12. $\rho(T)$ of Fe_{Tl}-2234.

Nevertheless, because of the number of different Fe sites coexisting in this structure, a more detailed analysis of the magnetic behavior is difficult to propose from these magnetization loops, and the magnetic structure will have to be determined by using neutron powder diffraction in order to explain the magnetic behavior and more particularly the low magnetization value and unusual T dependence variation of the coercive field. Figure 12 presents the resistivity curve and points toward a semiconducting like behavior, with $\rho \sim 800\ \Omega\cdot$cm at 300 K, and the activation energy is equal to 200 meV. These values are of the same order as the ones obtained for the Fe-2201,[22] the Fe_{Bi}-2212[24] and the ordered perovskite $Bi_{1/3}Sr_{2/3}FeO_{2.67}$[32] phases.

Discussion and Concluding Remarks. The Tl-doped strontium ferrite $Fe_2(Sr_{2-\epsilon}Tl_\epsilon)Sr_3Fe_4O_{14.65}$ exhibits an original 2234 structure. A first interesting point is the role played by thallium in the formation of this phase. The structural mechanisms that govern the stabilization of the different members of the family have been detailed elsewhere,[33] but it is clear that the presence of thallium is crucial for the stabilization of the phase since all attempts to synthesize the phase starting from nominal compositions $Fe_2(Sr_{2-\epsilon}A'_\epsilon)Sr_3Fe_4O_z$ (A′ being any $5d^{10}$ post transition cation) with $0 \leq \epsilon \leq 0.1$ failed.

On the bases of the general formula $Fe_2(Sr_{1.9}Tl_{0.1})Sr_3Fe_4O_{15.5-\delta/2-4y}$ and the experimental oxygen content (14.65 per unit), the Fe_{Tl}-2234 new phase can be described as the alternation along the $\vec{c}$ axis of a complex triple rock salt-type layer $[Fe_2(Sr_{1.9}Tl_{0.1})O_{3.4}]_\infty$ with a quadruple perovskite slice $[(SrFeO_{2.8})_4]_\infty$. The perovskite layers ($SrFeO_{2.8}$) are partially oxygen deficient. The uniform contrast observed at the level of the perovskite slice in the TEM images is consistent with a random distribution of about 10% of the oxygen vacancies in the basal planes of the octahedra. The amplitude of the modulation vector αa^* is correlated to the oxygen content located in between the two [FeO] layers of the complex double iron layer and can be directly compared to that of the reduced Fe-2201 $(Fe_2)(Sr)SrFeO_{6.4}$,[22,23] for which α decreases down to 0.4 (the as-synthesized Fe-2201 is characterized by an incommensurate modulation vector with $\alpha \approx 0.47$). However, in the latter compounds, exhibiting a single perovskite layer ($m = 1$), as well as for the Fe_{Bi}-2212[24] ($m = 2$ and $\alpha = 1/3$ for the as-synthesized sample), a centering of the modulated contrast is observed between two successive complex double iron layers. This translation of the position of the basic structural unit [(TBP)(TBP)], which generates a convex region in the double iron layer, is clearly visible in the two first structures, which are characterized by a thinner perovskite slice (Figure 5a and 5b). This translation is one way to accommodate the strain effect because of the alternation of convex and concave regions in the complex double iron layer. In these two examples, a lowering of the symmetry is observed with regard to the *Fmmm*-type subcell. In the Fe_{Tl}-2234, the perovskite layer is significantly thicker, so that the strain is accommodated and the symmetry of the subcell is retained. Such an effect of constrained relaxation by the perovskite layer can be simply observed in the defect perovskites $A_nB_nO_{3n-1}$. In the brownmillerite,[1] the orientation of the two tetrahedra alternates in successive layers leading to the conventional OTOT′ structure; in the higher n members, however, the rule is no longer respected and the tetrahedra commonly adopt the same orientation as OOT in the $n = 3$ member (see ref 34 for a review).

Note that the only nonstoichiometry effect detected in this material is the appearance of crystallographic shear planes, leading to the local formation of nanophases similar to those observed in the Pb-doped terrace structure.[30] The investigation of the Tl−Sr−Fe−O system will therefore be of interest to understand the role of the $6s^2$ lone pair in the stabilization of shear structures.

The present new phase belongs to a large family derived from the $Sr_4Fe_6O_{13-\delta}$ series, which is its first member. It opens the route to a large family of Fe_A-$(n-1)2(m-1)$m ferrites with general formula $Fe_2(A_2)Sr_{m-1}Fe_mO_{(3-y)m+(3.5-\delta/2)}$. The evidence of ferrimagnetic properties in this novel perovskite-related material is certainly a motivation to continue this research.

Acknowledgment. The authors acknowledge financial support from the European Union under the Framework 6 program under a contract for an Integrated Infrastructure Initiative. Reference 026019 ESTEEM. The authors thank Dr. O. Pérez for the fruitful discussion on modulated structures.

CM8014385

(32) Lepoittevin, C. Malo, S. Barrier, N. Nguyen N. Van Tendeloo G. and Hervieu. M. J. Solid State Chem. 2008, submitted.
(33) Lepoittevin, C. Ph.D. Thesis, University of Caen, France, Dec 4, 2006. Lepoittevin, C.; Malo, S.; van Tendeloo, G.; Hervieu, M. *J. Mater. Chem.* Submitted for publication.
(34) Mitchell, H. R. *Perovskites, modern and ancient*; Almaz Press: Thunder Bay, Ontario, 2002.